Article:
Sui, P, Sun, J, Hua, Y et al. (5 more authors) (2018) Effect of temperature and pressure on corrosion behavior of X65 carbon steel in water-saturated CO_2 transport environments mixed with H_2S. International Journal of Greenhouse Gas Control, 73. pp. 60-69. ISSN 1750-5836

https://doi.org/10.1016/j.ijggc.2018.04.003

Effect of temperature and pressure on corrosion behavior of X65 carbon steel in water-saturated CO_2 transport environments mixed with H_2S

Pengfei Sui[a], Jianbo Sun[a,*], Yong Hua[b], Huifeng Liu[a], Mingnan Zhou[a], Yucan Zhang[a], Jiahang Liu[a], Yong Wang[a]

[a] School of Mechanical and Electronic Engineering, China University of Petroleum, Qingdao 266580, PR China

[b] Institute of Functional Surfaces, School of Mechanical Engineering, University of Leeds, Leeds, LS2 9JT, United Kingdom

Abstract: The effect of temperature and pressure on corrosion behavior of X65 carbon steel in water-saturated supercritical CO_2 containing H_2S was studied to determine the role of H_2S on the corrosion product formation and corrosion mechanism. Weight loss measurements showed that the highest corrosion rate of 0.190 mm/year was recorded at 35 °C and 8 MPa. The presence of 1000 ppmv H_2S resulted in the corrosion products comprised of a double-layer structure in both supercritical and non-supercritical conditions. The results indicated that the presence of 1000 ppmv H_2S has significantly influenced on the corrosion mechanisms, corrosion product morphology and composition as well as promoted the precipitation of water based on thermodynamic model.

Key words: CO_2 transport; Carbon steel; Corrosion; H_2S; Thermodynamic model

1. Introduction

Greenhouse effect that leads to global warming has become a wide public concern, which mainly caused by CO_2 emission into the atmosphere. The large amount of CO_2 emission not only pollutes environment severely, but also gives rise to the threat of natural ecology. Therefore, reducing CO_2 emission is urgently awaited to be solved (Choi and Nesic, 2011a; Sim et al., 2013).

Carbon capture and storage (CCS) technology is considered to be one of the main options for achieving significant reduction in greenhouse gas emissions. The

* Corresponding author. Tel.: +86 532 86983503-8625; fax: +86 532 86983300.
E-mail address: sunjianbo@upc.edu.cn

process of CCS involves mainly three stages: CO_2 capture, CO_2 transport, and CO_2 injection into geological reservoirs or the use of enhanced oil recovery purpose. The transport of large amount of CO_2 is either in liquid or supercritical state. The critical temperature and pressure for supercritical CO_2 are 31.1 °C and 7.38 MPa (Gale and Davison, 2004; Boot-Handford et al., 2013). The most common material for the transport of large amount of CO_2 is carbon steel due to its low cost and mechanical properties. Nowadays, there are over 6,500 km CO_2 transport pipelines in the world and most of the pipelines are made of the carbon steels, such as X65 and X70 carbon steels (Dooleya et al. 2009). However, there will be a large amount of H_2S impurity in the captured CO_2 by using pre-combustion capture technology. Also, the captured CO_2 from coal-fired power plants unavoidably contains impurities like NO_x, SO_x, H_2O, O_2 and H_2S (Visser et al., 2008; Xiang et al., 2017a), which are primary cause for pipeline corrosion, and pose threat to the pipeline integrity.

Up to now, there are many studies on the corrosion behaviors of carbon steels in supercritical CO_2 system containing impurities under various conditions. Table 1 summarizes the recent research on supercritical CO_2 corrosion (Brown et al., 2014; Choi and Nesic, 2011; Choi et al., 2015; Farelas et al., 2013; Hua et al., 2014; Sun et al., 2017; Xiang et al., 2013a, 2013b; Xu et al., 2016a, 2016b). Among these researches, some investigated the corrosion behavior of carbon steel with the change of certain pressure or temperature. Choi and Nesic (2011) studied the corrosion behavior of X65 steel in supercritical CO_2 system and draw the conclusion that the corrosion rates of carbon steel in the CO_2-saturated water were very high (about 18-20 mm/y) but did not significantly change with pressure from 4 to 8 MPa. Whereas, the research results of Xu et al. (2016a) showed that the general and localized corrosion attack were higher at 8 MPa than those at 10 MPa for a constant temperature of 50 °C, with water contents ranging from 1600 ppm to 2600 ppm, but lower at a water content of 3000 ppm. Xiang et al. (2013a) found that the corrosion rate increased with increasing in temperature and then started to decline at the highest corrosion rate at 75 °C in supercritical CO_2-H_2O-SO_2-O_2 system. Brown et al. (2014) investigated the corrosion behavior of X65 steel at 4 °C and 50 °C under the pressure of 10 MPa to

define a safe operating window for dense phase CO_2 containing various impurities. Hua et al. (2014) studied the effect of temperature on the critical water content of X65 steel and the results showed that the general corrosion rates at 35 °C was much higher than that at 50 °C when the experimental pressure was 8 MPa containing 3437 and 3400 ppm water respectively. Compared with several research results, it should be noted that corrosion rate changes variously under different temperature and pressure. However, among their studies, the effect of temperature or pressure change the on corrosion behavior of carbon steel has not been reported. Considering the actual transport conditions, CO_2 pipelines are generally buried under ground (Zhang et al., 2006), where the fluctuation of temperature and pressure is inevitable because of the different geographical environments (Freeman et al., 2003). Besides, there is a problem of pressure drop during long distance pipeline transportation in the presence of impurities above, which may change CO_2 phase under different conditions (Peletiri et al., 2017).

The recent studies on the supercritical CO_2 corrosion mainly focus on impurities such as O_2, SO_2, mixed CO_2 with sulfurous acid or the mixture with H_2S (Hua et al., 2015a, 2015b, 2017; Sun et al., 2016a, 2016b, 2016c; Tang et al., 2017;Wei et al., 2016a, 2016b; Xiang et al., 2011, 2013a, 2013b, 2017b). However, the effect of H_2S as impurity on the corrosion behavior of CO_2 transmission pipeline has rarely been reported. The present studies show that small amount of H_2S in the supercritical CO_2 phase can change the adsorbability of H_2O on the steel surface (Wei et al., 2016a) and form a weak acid when dissolved in water, which can be the origin of corrosion (Sun et al., 2016a, 2016b). Due to the high toxicity of H_2S, the existed quality standard of CO_2 transmission on the limitation of H_2S concentration is based on the health and safety considerations (Visser et al., 2008). Recent work done by Sun et al. (2016b) suggested that trace H_2S could accelerate the corrosion process under supercritical CO_2 environment. The results of Choi et al. (2015) and Wei et al. (2016a) also showed the potential corrosion risk with the H_2S mixture in CO_2 transport pipelines. However, it is clear that some questions still remain on the role of H_2S in high pressure of CO_2 stream. One issue is the level of corrosion and the change in temperature and pressure

on the corrosion behavior (particularly CO_2 phase change, liquid and supercritical CO_2 phase). Furthermore, the other is to investigate the H_2S influence on the formation of FeS and $FeCO_3$ as well as the material degradation rate.

The aim of this work is to understand the effect of temperature and pressure on the corrosion behavior of X65 carbon steel in water-saturated CO_2-H_2O-H_2S environments. The conditions considered include: water-saturated liquid CO_2 (temperature and pressure are 25 °C, 8 MPa and 35 °C, 6 MPa) and water-saturated supercritical CO_2 (temperature and pressure are 35 °C, 8 MPa, 35 °C, 10 MPa and 50 °C, 8 MPa) phase. The general corrosion rates in the system were determined through weight loss measurements. The morphology and composition of corrosion scales were characterized by Scanning Electron Microscope (SEM), Electron Probe Micro-Analyzer (EPMA) and X-ray Diffraction (XRD). The water solubility was calculated by establishing thermodynamic model based on Redlich-Kwong equation of state (RK-EOS) in CO_2-H_2O-H_2S system. Accordingly, the impact of temperature and pressure change on corrosion rate variation was evaluated by the formula put forward in the work.

2. Materials and methods

2.1 Materials and preparation

The specimens were machined into a size of 35 mm ×15 mm ×3 mm. The chemical composition (wt %) of the X65 steel is: 0.06 % C, 0.288 % Si, 1.52 % Mn, 0.012 % P, 0.003 % S, 0.048 % Cr, 0.008 % Ni, 0.178 % Mo, 0.007 % Cu, 0.057 % Al, 0.031 % V and Fe balance. The microstructure of the material is provided in Fig. 1a. A ferritic-pearlitic microstructure is observed for X65 carbon steel. As shown in Fig. 1b, there was no deformation of grains in the surface region after the specimens machined with certain size requirements. Before the experiment, all the specimens were wet-grinding up to 1000 grit SiC paper, and then rinsed with deionized water, acetone and dried with cold air. The samples were put in a desiccator until weighed using an electronic balance to a precision of 0.1 mg before the experiments.

2.2 Corrosion experiments

The corrosion experiments were carried out in an autoclave to investigate the corrosion rate and morphology of corrosion product formed on carbon steel surface in supercritical CO_2 system containing 1000 ppmv H_2S. The schematic diagram of the whole system is shown in Fig. 2. The apparatus mainly consists of CO_2/H_2S gas mixture cylinder, a booster pump, a 3 liter capacity autoclave, a controller and a waste gas treatment device. The controller is used for the measurement of temperature and pressure with the precision of 0.1 °C and 0.01 MPa. The entire test matrix is listed in Table 2. According to Spycher et al. (2003), the water concentration reach the saturated point at the test conditions varies between 1711 ppm and 3946 ppm (dissolved H_2O in CO_2 in a 3 L autoclave is between 0.334 g and 3.663 g). Thus, 10 g of water was introduced into the autoclave for the water-saturated environments.

Before corrosion experiments, the deionized water was deoxygenized by pure N_2 for 12h. In each test, four parallel specimens were hung on the polytetrafluoroethylene (PTFE) holder. When the autoclave was sealed, purging CO_2 was introduced to remove the air for 2 h. After the autoclave was heated to the adjusted temperature, CO_2 or CO_2/H_2S mixture gas was injected into the autoclave with a booster pump to reach the required pressure. All the tests were carried out under static conditions.

2.3 Weight loss tests

After the corrosion test, the specimens were rinsed with deionized water, dried thoroughly and photographed. Three specimens were chemical cleaned to remove the corrosion products. The chemical solution consisted of hydrochloric acid (100 ml), hexamethylenetetramine (5 g) and deionized water (900 ml) at room temperature (ASTM Standard G1-03, 2011). And the general corrosion rate was calculated according to the following equation (ASTM Standard G31-72, 2004):

$$V_{CR} = \frac{87600\Delta W}{S\rho t} \tag{1}$$

where V_{CR} is the general corrosion rate, mm/y; ΔW is the weight loss, g; S is the exposed surface area of specimen, cm^2; ρ is the density of specimen, g/cm^3; t is the

exposure time, h; 87600 is the unit conversion constant.

3. Results

3.1 General corrosion rate

Fig. 3 shows the general corrosion rates calculated from the mass loss data of X65 steels exposed to the water-saturated liquid CO_2 and supercritical CO_2 with the presence of 1000 ppmv H_2S at different temperature and pressure. Fig. 3a shows the general corrosion rates of X65 steel under different temperatures at the same pressure of 8 MPa. It can be seen that when the temperature was 35 °C, the corrosion rate reached the highest value of 0.190 mm/year. When the temperature increased from 35 °C to 50 °C, it resulted in the corrosion rate of X65 steel reduced to 0.032 mm/year. The general corrosion rate of 0.095 mm/year was recorded at 27 °C and 8 MPa. The results (Fig. 3b) show that the corrosion rate of 0.017, 0.190 and 0.073 mm/year were at 6, 8 and 10 MPa respectively when maintaining the temperature at 35 °C. It is interesting to note that the corrosion rate at 27 °C and 8 MPa in liquid CO_2 phase is higher than that of 50 °C, 8 MPa and 35 °C, 10 MPa in supercritical CO_2 phase.

3.2 Macroscopic and SEM/EPMA surface analysis of corrosion scales

Fig. 4 shows the macroscopic images of X65 steel before and after being corroded for 72 h in water-saturated liquid/supercritical CO_2 with the presence of 1000 ppmv H_2S. It can be seen that all steel samples became discolored. The most corrosive condition is at 35 °C and 8 MPa in accordance with the highest corrosion rate of 0.190 mm/year recorded in Fig. 3. All the corroded areas are identified within each of the SEM images in Fig. 5 and 7.

All the samples were covered with corrosion products on the entire surface as shown in Fig. 5. EPMA analysis (Table 3) in different regions identified in the figure showed that the corrosion products were rich in sulfur element and mainly contained 49.14 % Fe and 50.86 % S respectively in region B (Fig. 5a). The increase in temperature from 27 °C to 35 °C caused more serious corrosion of the sample (Fig. 5b). The observed corrosion scale morphology on the surface indicated the presence of cracked sulfur-containing layer. When the temperature and pressure reached 50 °C,

8 MPa, the corrosion of sample surface became milder than that at lower temperature and polish mark was still visible as shown in Fig. 5c. Similar corrosion products were observed at 35 °C, 6 MPa. Final test was performed at temperature and pressure of 50 °C and 10 MPa and the corrosion products also contained high quantities of sulfur element. Fig. 6 provided XRD pattern of samples exposed to the water-saturated supercritical CO_2 condition with the presence of 1000 ppmv H_2S at various temperature and pressure. The results indicated that the addition of 1000 ppmv H_2S resulted in the formation of FeS crystals on the surface. $FeCO_3$ crystals were also detected on the surface from the XRD pattern. Similar observation was reported by Choi et al. (2015) and Sun et al. (2016a).

SEM images and EPMA elemental maps of cross sections of X65 carbon steels after corrosion tests are provided in Fig. 7. The results showed that the corrosion products contained high levels of sulfur element in all test conditions. It is interesting to noting that a double-layer structure can be clearly observed at 27 °C and 8 MPa, and EPMA mapping of the cross-section of X65 indicated that high level of S was detected at the outer layer and the inner layer were comprised of Fe and O (Fig. 7a). XRD pattern showed that the corrosion scales contained mainly FeS and $FeCO_3$ (Fig. 6a). The EPMA analysis (Table 4) indicated that the outer layer contained Fe and S in accordance with XRD pattern. According to EPMA analysis of region A in Fig 7a, the outer layer was FeS with the atom ratios of Fe and S near 1:1. While the inner layer contained much C and O compared to outer layer, it can be indicated that the composition of inner layer were FeS and $FeCO_3$ based on atom percentage of region B. Such corrosion products were also observed by Sun et al. (2016b) and Choi et.al (2015). The thickness of the corrosion product was near 12 μm at 27 °C and 8 MPa. And it decreased from 30 μm to 5 μm as increasing the temperature from 35 °C to 50 °C. A thin corrosion product layer observed on the surface sample at 35 °C and 6 MPa, which was rich in sulfur as showed in Fig. 7d. The corrosion product layer at 35 °C and 10 MPa had similar thickness and became more non-uniform in thickness cross the steel surface.

Fig. 8 shows the SEM images with surface roughness of X65 steel (after removal

of the corrosion scales) at various temperature and pressure. It is interesting to note that the surface was corroded severely at 35 °C, 8 MPa (Fig. 8b) in agreement with the highest corrosion rate of 0.190 mm/year as shown in Fig. 3. Comparing two noncritical conditions, the sample surface at 27 °C and 8 MPa (Fig. 8a) was corroded more severely than that at 35 °C and 6 MPa (Fig. 8b). The surface roughness (Ra) was the surface arithmetic average of absolute values based on the vertical deviations of the roughness profiles from the mean line obtained by using 3D surface profiler. The original surface roughness was about 147 nm (approximately 0.15 μm).The results indicated that the highest value of Ra of 2.70 μm was measured for the sample at 35 °C and 8 MPa. The slightly corroded sample surfaces at 35 °C, 6 MPa (Fig. 8d) and 50 °C, 8 MPa (Fig. 8c) indicated smaller Ra values and the polishing lines were still visible for those two conditions.

4. Discussions

4.1 Effect of temperature and pressure change on X65 steel corrosion behavior

In order to investigate the effect of the temperature and pressure on the corrosion behavior of X65 in water-saturated CO_2, the following formulas (Eqs. (2) and (3)) were used to calculate the corrosion rates as a function of temperature and pressure. Where CR is corrosion rate, mm/y; ΔT is the difference in temperature, °C; ΔP is the difference in pressure, MPa; ΔCR_T is the difference in corrosion rate with temperature, mm/y • °C $^{-1}$; ΔCR_P is the difference in corrosion rate with pressure, mm/y • MPa^{-1}.

$$\Delta CR_T = \frac{CR_1 - CR_2}{\Delta T} \tag{2}$$

$$\Delta CR_P = \frac{CR_1 - CR_2}{\Delta P} \tag{3}$$

Fig. 9 shows the corrosion rates varied with temperature and pressure. It can be seen that the change of temperature in different parts had the same effect on corrosion rate changes of X65 steel at 0.01 mm/y • °C $^{-1}$. However, as the pressure increased

from 6 MPa to 8 MPa, the corrosion rate change was nearly 0.09 mm/y • MPa^{-1}, around 30 % higher than the value for the change from 8 MPa to 10 MPa. The results indicated that the change of temperature had less effect than pressure change in the test system. Besides, with the increase of pressure, the corrosion rate variation was decreased accordingly.

4.2 Effect of temperature and pressure on thermodynamic property of supercritical CO_2-H_2O-H_2S system

4.2.1 The effect of temperature and pressure on solubility of water in CO_2 with H_2S impurity

Spycher et al. (2003) established the thermodynamic model of CO_2-H_2O mixture system. The mutual solubility of H_2O and CO_2 can be calculated by the following equations:

$$x_{CO_2} = \frac{\phi_{CO_2}(1 - y_{H_2O})P_{tot}}{55.508K^0_{CO_2(g)}} \exp\left(-\frac{(P - P^0)\overline{V}_{CO_2}}{RT}\right) \quad (4)$$

$$y_{H_2O} = \frac{K^0_{H_2O} a_{H_2O}}{\phi_{H_2O} P_{tot}} \exp\left(\frac{(P - P^0)\overline{V}_{H_2O}}{RT}\right) \quad (5)$$

For a system where H_2O and CO_2 are the only two components, x_{H_2O} is directly calculated as $1 - x_{CO_2}$. At the pressures and temperatures, the solubility of CO_2 is sufficiently small such that Raoult's law can be used to set the water activity (a_{H_2O}) equal to its mole fraction in the water phase (x_{H_2O}).

$$a_{H_2O} = 1 - x_{CO_2} \quad (6)$$

In the above equations, P_{tot} is the total pressure; P is the partial pressure; P^0 is the reference pressure; R is the gas constant; T is the temperature; $\overline{V}_{H_2O}$ is the average partial molar volume of pure water; $\overline{V}_{CO_2}$ is the average partial molar volume of CO_2; K is the true equilibrium constants; ϕ is the fugacity coefficient. These constants can be obtained from literature (Choi and Nesic, 2011; Spycher et al., 2003).

Zirrahi et al. (2010) studied the prediction of water content of sour and acid gases. Based on Spycher's thermodynamic model, the water content can be calculated according to the following equations in CO_2-H_2O-H_2S-CH_4-brine system:

$$a_{H_2O} = 1 - x_{H_2S} - x_{CO_2} - x_{CH_4} - x_{salt} \tag{7}$$

$$y_{H_2O} = \frac{K^0_{H_2O}(1 - x_{H_2S} - x_{CO_2} - x_{CH_4} - x_{salt})}{\phi_{H_2O} P_{tot}} \exp\left(\frac{(P - P^0)\overline{V}_{H_2O}}{RT}\right) \tag{8}$$

Based on the modified RK-EOS (Choi and Nesic, 2011a), the solubility thermodynamic model in CO_2-H_2O-H_2S system can be developed as follow:

$$y_{H_2O} = \frac{K^0_{H_2O}(1 - x_{H_2S} - x_{CO_2})}{\phi_{H_2O} P_{tot}} \exp\left(\frac{(P - P^0)\overline{V}_{H_2O}}{RT}\right) \tag{9}$$

$$a_{H_2O} = 1 - x_{H_2S} - x_{CO_2} \tag{10}$$

where x is the mole fraction of acid gases in aqueous phase. To avoid iteration, the solubility of CO_2 and H_2S can be calculated by using the methods of Duan et al. (Duan et al., 1992, 2003, 2007, 2008).

Fig. 10a shows the calculated solubility of water in CO_2 as a function of temperature and pressure with the presence of 1000 ppmv H_2S. The solubility of water decreased first and then increased with the rising temperature. Similar observations have been reported by Choi and Nesic (2011), who also calculated the solubility of water in CO_2 as a function of temperature and pressure. They reported that with the increase of the temperature and pressure to a certain point, the solubility of water decreased gradually and then, sharply increased near the critical pressure point. The additional of 1000 ppmv H_2S into the CO_2-H_2O system at 35 °C and 8 MPa results in no significant reducing the solubility of water in CO_2 as shown in Fig. 10b. Hua et al. (2015b) investigated the corrosion rate of X65 steel in supercritical CO_2-H_2O system at 35 °C and 8 MPa containing 10 g H_2O for 48 hours, and the general corrosion rate was 0.1 mm/year. While in this experiment, the corrosion rate of 0.190 mm/year was recorded for samples exposed to the water-saturated supercritical CO_2 at 35 °C and 8 MPa with the presence of 1000 ppmv H_2S. This observation suggests that the presence of 1000 ppmv H_2S has the ability to influence

the corrosion kinetics. The addition of 1000 ppmv H_2S can promote the corrosion process and take the leading role during the degradation process.

Refer to the XRD pattern in Fig. 6, both FeS and $FeCO_3$ were detected on the sample exposed to the water-saturated supercritical CO_2 environment in the presence of 1000 ppmv H_2S at various temperature and pressure. The main corrosion process can be summarized, as discussed by (Choi et al., 2015; Sun et al., 2016a; Wei et al., 2016b; Zheng et al., 2014) provided in Fig.11. Initially, supercritical CO_2 and H_2S impurity dissolved into water and dissociated into different ions (H^+, CO_3^{2-}, HCO_3^-, HS^-, S^{2-}) and some H_2S would react with iron directly. The dissolution of steel was the main anodic reaction to form Fe^{2+}. The addition of H_2S provided additional cathodic reaction pathway for corrosion (Abelev et al., 2009).

4.2.2 The relationship between corrosion behavior and system density

When finished corrosion test, there was a phenomenon should be noted. As Fig. 12 shows, the test water froze after exhausting the gases at some test conditions. The process of exhausting gases would take away a great deal of heat that caused the water frozen. However, this phenomenon had not occurred in all test conditions, which only appeared at 27 °C, 8 MPa and 35 °C, 10 MPa.

Considering the physicochemical property of CO_2, the corrosion system gas density was calculated according to Duan et al., (2008), seen in Table 5. The results showed that the two frozen conditions had higher CO_2 densities which are over 700 kg/m^3 than other conditions. According to the physical absorption formula shown as Eq. (11), the water content was the same in all tests, the greater mass of CO_2, the more heat it took away when exhausting gases.

$$Q_{absorption} = Cm\Delta t \tag{11}$$

Where $Q_{absorption}$ is the absorbed heat; C is the specific heat capacity; m is the mass; Δt is the temperature change.

Fig. 13 shows the corrosion rates and system densities under different test conditions. The change of system densities had the same trend of corrosion rates except at 35 °C, 8 MPa. When the corrosion rate reached the minimum at 0.032

mm/year, the system density was also at the lowest value around 159 kg/m^3. While with the increase or decrease of corrosion rates, the system density changed accordingly. However, when at 35 °C and 8 MPa, the corrosion rate was at peak with median density of system. Based on the supercritical CO_2 fluid characteristic, the self-diffusion coefficient, viscosity and thermal conductivity change dramatically when temperature and pressure are near the critical point. It may be the principal factor that leads to severe corrosion.

According to the above results, corrosion rates of X65 steel changed with the system density in a similar trend, which indicated the relation between them. While the test condition is around critical point, supercritical CO_2 has special properties that the relationship between density and corrosion rate is not well fitted at that condition.

5. Conclusions

In this work, the effect of temperature and pressure on corrosion behavior of X65 steel was investigated in water-saturated CO_2-H_2O-H_2S system. The X65 carbon steels formed double-layer structured corrosion products in both supercritical and non-supercritical state. When the temperature and pressure were at 35 °C and 8 MPa, the corrosion rate reached the maximum 0.190 mm/year.

The thermodynamic model in CO_2-H_2O-H_2S system was developed and showed that the addition of H_2S impurity can promote the precipitation of water, which can accelerate corrosion process and increase the corrosion rate of X65 steel. The effect of temperature change on corrosion rate variation had less impact than the change of pressure. What's more, the corrosion rate change had the same trend with the system density change except the condition when it was around the critical temperature and pressure of CO_2.

Acknowledgements

This work was supported by National Natural Science Foundation of China (No. 51471188) and Natural Science Foundation of Shandong Province (No. ZR2014EMM002).

References

ASTM Standard G31-72, 2004. Standard Practice for Laboratory Immersion Corrosion Testing of Metals. ASTM International, West Conshohocken, PA.

ASTM Standard G1-03, 2011. Standard Practice for Preparing, Cleaning, and Evaluating Corrosion Test Specimens. ASTM International, West Conshohocken, PA.

Abelev, E., Ramanarayanan, T.A., Bernasek, S.L., 2009. Iron corrosion in CO_2/brine at low H_2S concentrations: an electrochemical and surface science study. J. Electrochim. Soc. 156, 331-339.

Boot-Handford, M. E., Abanades, J. C., Anthony, E. J., Blunt, M. J., Brandani, S., 2013. Carbon capture and storage update. Energy Environ. Sci. 7, 130-189.

Brown, J., Graver, B., Gulbrandsen, E., Dugstad, A., Morland, B., 2014. Update of DNV recommended practice RP-J202 with focus on CO_2 corrosion with impurities. Energy Procedia 63, 2432-2441.

Choi, Y.S., Nesic, S., 2011. Determining the corrosive potential of CO_2 transport pipeline in high pCO_2-water environments. Int. J. Greenh. Gas Control 5, 788-797.

Choi, Y. S., Hassani, S., Vu, T. N., Nesic, S. A., Abas, Z. B., 2015. Effect of H_2S on the corrosion behavior of pipeline steels in supercritical and liquid CO_2 environments. Corrosion/2015. NACE, Houston, TX Paper No. 5927.

Dooleya, J. J., Dahowskib, R.T., Davidsonb, C., 2009. Comparing existing pipeline networks with the potential scale of future U.S. CO_2 pipeline networks. Energy Procedia 1, 1595-1602.

Duan, Z.H., Møller, N., Greenber, J., Weare, J.H., 1992. The prediction of methane solubility in natural waters to high ionic strength from 0 to 250°C and from 0 to 1600 bar. Geochim. Cosmochim. Acta 56, 1451-1460.

Duan, Z.H., Sun, R., 2003. An improved model calculating CO_2 solubility in pure water and aqueous NaCl solutions from 273 to 533 K and from 0 to 2000 bar. Chem. Geol. 193, 257-271.

Duan, Z.H., Sun, R., Liu, R., Zhu, C., 2007. An accurate thermodynamic model for the calculation of H_2S solubility in pure water and brines. Energy Fuels 21, 2056-2065.

Duan, Z.H., Hu, J.W., Li, D.D., Mao, S.D., 2008. Densities of the CO_2-H_2O and CO_2-H_2O-NaCl systems up to 647K and 100MPa. Energy Fuels 22, 1666-1674.

Farelas, F., Choi, Y.S., Nesic, S., 2013. Corrosion behavior of API 5L X65 carbon steel under supercritical and liquid carbon dioxide phases in the presence of water and sulfur dioxide. Corrosion 69, 243-250.

Freeman, D.J., Findlay, D.A., Bamboat, M., Davison, J., Forbes, I., 2003. Costs and performance of CO_2 and energy transmission. Proceedings of the 6th International Conference on Greenhouse Gas Reduction Technologies, Elsevier Science, London, UK, 1131-1136.

Gale, J., Davison, J., 2004. Transmission of CO_2-safety and economic considerations. Energy 29, 1319-1328.

Hua, Y., Barker, R., Neville, A., 2014. Effect of temperature on the critical water content for general and localized corrosion of X65 carbon steel in the transport of supercritical CO_2. Int. J. Greenh. Gas Control 31, 48-60.

Hua, Y., Barker, R., Neville, A., 2015a. The influence of SO_2 on the tolerable water content to avoid pipeline corrosion during the transportation of supercritical CO_2. Int. J. Greenh. Gas Control 37, 412-423.

Hua, Y., Barker, R., Neville, A., 2015b. The effect of O_2 content on the corrosion behavior of X65 and 5Cr in water-containing supercritical CO_2 environments. Appl. Surf. Sci. 356, 499-511.

Hua, Y., Jonnalagadda, R., Zhang, L., Neville, A., Barker, R., 2017. Assessment of general and localized corrosion behavior of X65 and 13Cr steels in water-saturated supercritical CO_2 environments with SO_2/O_2. Int. J. Greenh. Gas Control 64, 126-136.

Ma, H., Cheng, X., Li, G., Chen, S., Quan, Z., Zhao, S., Niu, L., 2000. The influence of hydrogen sulfide on corrosion of iron under different conditions. Corros. Sci. 42, 1669-1683.

Peletiri, S. P., Rahmanian, N., Mujtaba, I. M., 2017. Effects of impurities on CO_2 pipeline performance. Chemical Engineering Transactions 57, 355-360.

Sim, S., Cole, I. S., Bocher, F., Corrigan, P., Gamage, R.P., Ukwattage, N., Birbilis, N., 2013. Investigating the effect of salt and acid impurities in supercritical CO_2 as relevant to the corrosion of carbon capture and storage pipelines. Int. J. Greenh. Gas Control 17, 534-541.

Sun, J.B., Sun, C., Zhang, G.A., Li, X.D., Zhao, W.M., Jiang, T., Liu, H.F., Cheng, X.K., Wang, Y., 2016a. Effect of O_2 and H_2S impurities on the corrosion behavior of X65 steel in water-saturated supercritical CO_2 system. Corros. Sci. 107, 31-40.

Sun, C., Sun, J.B., Wang, Y., Lin, X.Q., Li, X.D., Cheng, X.K., Liu, H.F., 2016b. Synergistic effect of O_2, H_2S and SO_2 impurities on the corrosion behavior of X65 steel in water-saturated supercritical CO_2 system. Corros. Sci. 107, 193-203.

Sun, C., Wang, Y., Sun, J.B., Lin, X.Q., Li, X.D., Liu, H.F., Cheng, X.K., 2016c. Effect of impurity on the corrosion behavior of X65 steel in water-saturated supercritical CO_2 system. J. Supercrit. Fluids 116, 70-82.

Sun C., Sun, J.B., Wang, Y., Sui, P.F., Lin, X.Q., Liu, H.F., Cheng, X.K., Zhou, M.N., 2017. Effect of impurity interaction on the corrosion film characteristics and corrosion morphology evolution of X65 steel in water-saturated supercritical CO_2 system. Int. J. Greenh. Gas Control 65, 117-127.

Spycher, N., Pruess, K., Ennis-King, J., 2003. CO_2-H_2O mixtures in the geological sequestration of CO_2. I. Assessment and calculation of mutual solubilities from 12 to 1000 ˚C and up to 600 bar. Geochim. Cosmochim. Acta 67, 3015-3031.

Tang, Y., Guo, X.P., Zhang, G.A., 2017. Corrosion behavior of X65 carbon steel in supercritical-CO_2, containing H_2O and O_2 in carbon capture and storage (CCS) technology. Corros. Sci. 118, 118-128.

Visser, E.D., Hendriks, C., Barrio, M., Mølnvik, M. J., Koeijer, G. D., Liljemark, S., Gallo, Y. L., 2008. Dynamis CO_2 quality recommendations. Int. J. Greenh. Gas Control 2, 478-484.

Wei, L., Pang, X.L., Gao, K.W., 2016a. Effect of small amount of H_2S on the

corrosion behavior of carbon steel in the dynamic supercritical CO_2 environments. Corros. Sci. 103, 132-144.

Wei, L., Pang, X.L., Gao, K.W., 2016b. Corrosion of low alloy steel and stainless steel in supercritical $CO_2/H_2O/H_2S$ systems. Corros. Sci. 111, 637-648.

Xiang, Y., Wang, Z., Xu, C., Zhou, C.C., Li, Z., Ni, W.D., 2011. Impact of SO_2 concentration on the corrosion rate of X70 steel and iron in water-saturated supercritical CO_2 mixed with SO_2. J. Supercrit. Fluids 58, 286-294.

Xiang, Y., Wang, Z., Li, Z., Ni, W.D., 2013a. Effect of temperature on corrosion behavior of X70 steel in high pressure $CO_2/SO_2/O_2/H_2O$ environments. Corros. Eng. Sci. Technol. 48, 121-129.

Xiang, Y., Wang, Z., Li, Z., Ni, W. 2013b. Effect of exposure time on the corrosion rates of X70 steel in supercritical $CO_2/SO_2/O_2/H_2O$ environments. Corrosion 69, 251-258.

Xiang, Y., Xu, M.H., Choi, Y.S., 2017a. State-of-the-art overview of pipeline steel corrosion in impure dense CO_2 for CCS transportation: mechanisms and models. Corros. Eng. Sci. Technol. 52, 485-509.

Xiang, Y., Li, C., Long, Z.W., Guan, C.Y.Wang, W., Hesitao, W. 2017b. Electrochemical behavior of valve steel in a CO_2/sulfurous acid solution. Electrochim. Acta 258, 909-918.

Xu, M., Li, W., Zhou, Y., Yang, X.X., Wang, Z., Li, Z., 2016a. Effect of pressure on corrosion behavior of X60, X65, X70, and X80 carbon steels in water-unsaturated supercritical CO_2 environments. Int. J. Greenh. Gas Control 51, 357-368.

Xu, M., Zhang, Q., Yang, X. X., Wang, Z., Liu, J., Li, Z. 2016b. Impact of surface roughness and humidity on X70 steel corrosion in supercritical CO_2, mixture with SO_2, H_2O, and O_2. J. Supercrit. Fluids 107, 286-297.

Zhang, Z.X., Wang, G.X., Massarotto, P., Rudolph, V., 2006. Optimization of pipeline transport for CO_2 sequestration. Energy Convers. Manage. 47, 702-715.

Zheng, Y.G., Brown, B., Nešić, S., 2014. Electrochemical study and modeling of H_2S corrosion of mild steel. Corrosion 70, 351-365.

Zirrahi, M., Azin, R., Hassanzadeh, H., Moshfeghian, M., 2010. Prediction of water content of sour and acid gases. Fluid Phase Equilibr. 299, 171-179.

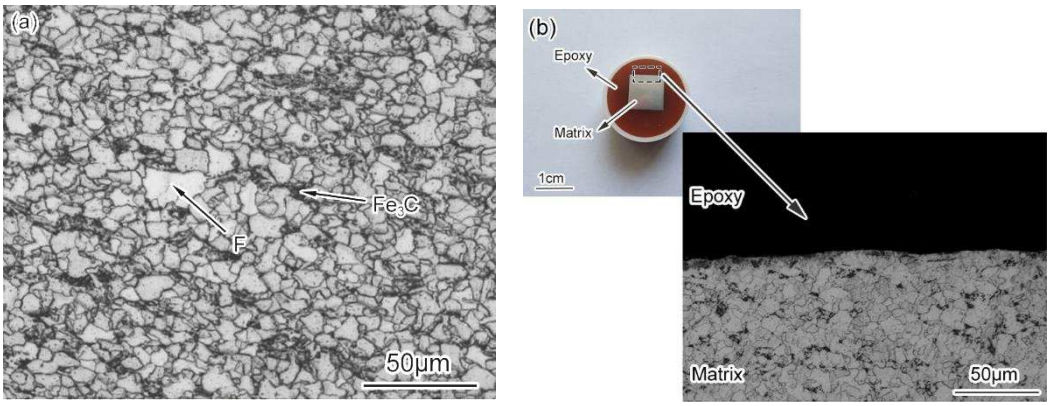

Fig.1. Optical microstructure of X65 steel.

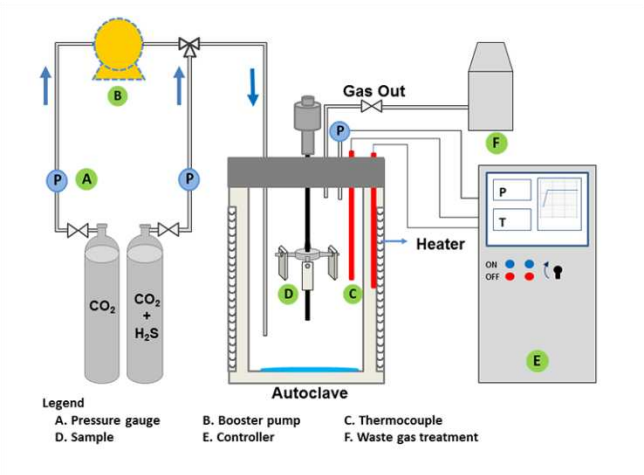

Fig.2. Schematic diagram of the apparatus for the corrosion test.

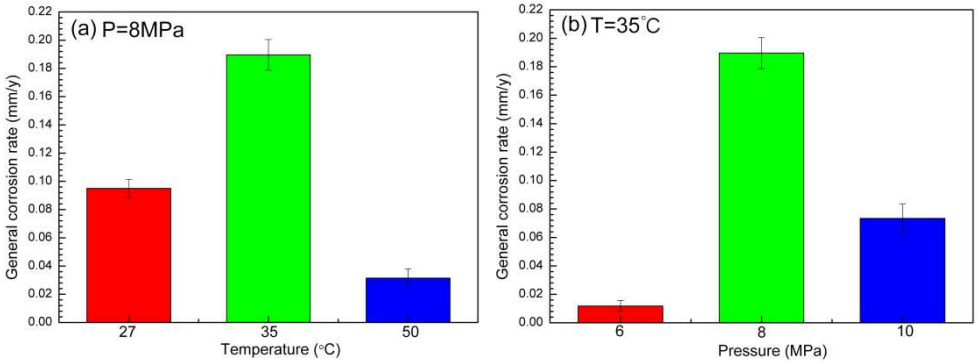

Fig.3. Corrosion rate of X65 steel exposed to water-saturated supercritical CO_2 containing 1000 ppmv H_2S impurity for 72 h at different conditions: (a) 8 MPa with different temperatures; (b) 35 °C with different pressures.

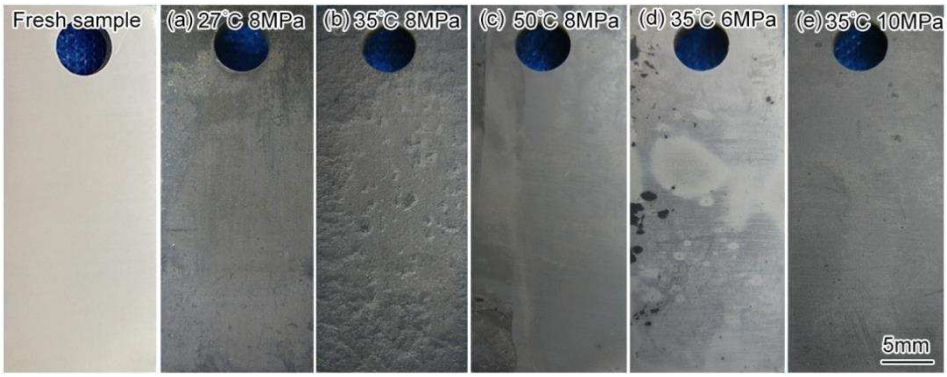

Fig.4. Macroscopic morphologies of corrosion scales on X65 steels exposed to water-saturated supercritical CO_2 system with 1000 ppmv H_2S impurity for 72 h at different conditions: fresh sample, (a) 27 °C, 8 MPa; (b) 35 °C, 8 MPa; (c) 50 °C, 8 MPa; (d) 35 °C, 6 MPa; (e) 35 °C, 10 MPa.

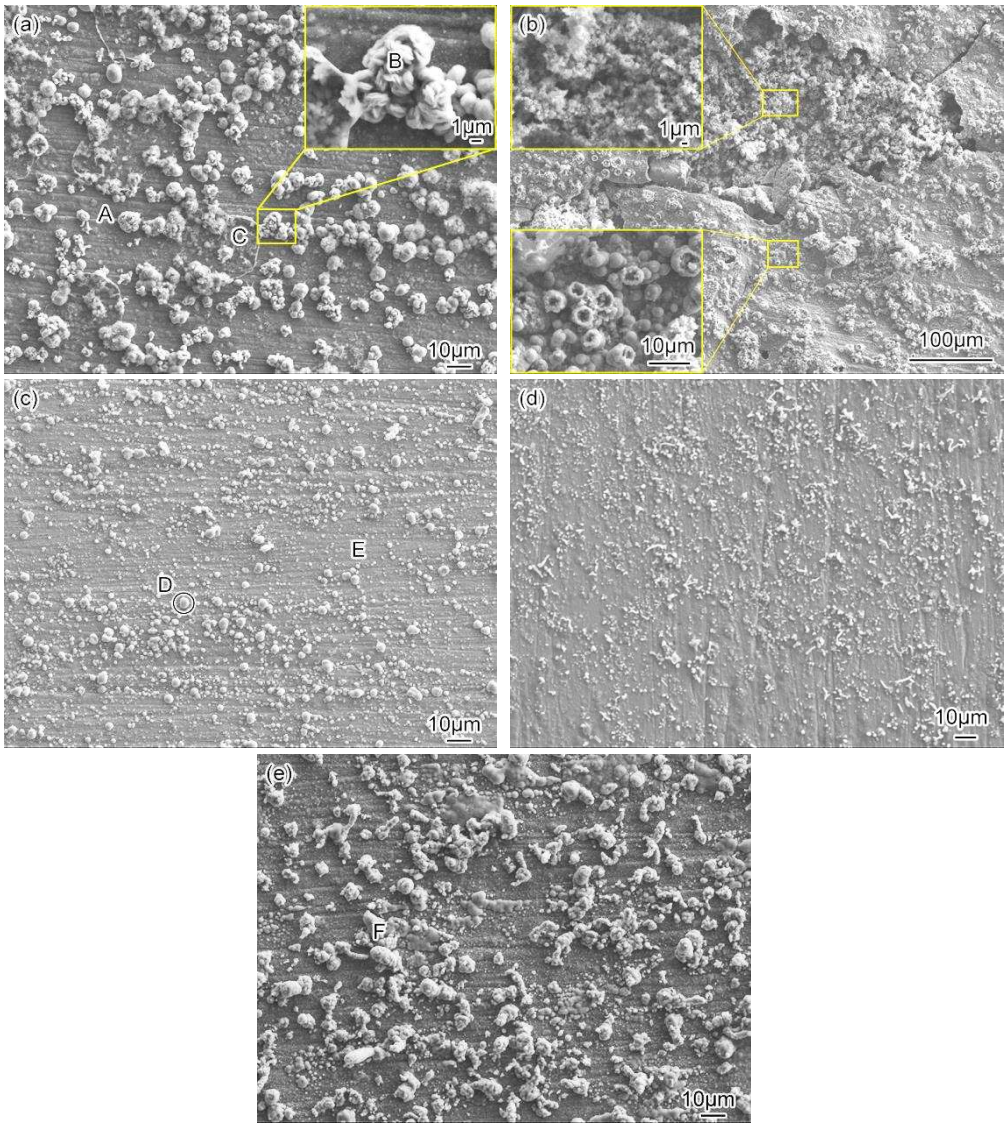

Fig.5. SEM surface morphologies of corrosion scales on X65 steels after 72 h in water-saturated supercritical CO_2 system containing 1000 ppmv H_2S impurity: (a) 27 °C, 8 MPa; (b) 35 °C, 8 MPa; (c) 50 °C, 8 MPa; (d) 35 °C, 6 MPa; (e) 35 °C, 10 MPa.

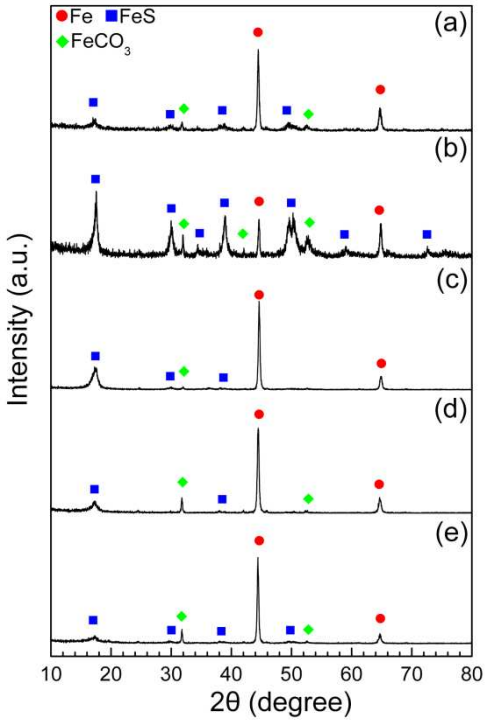

Fig.6. XRD spectra of corrosion scales on X65 steels after corrosion for 72 h in water-saturated supercritical CO_2 system containing 1000 ppmv H_2S impurity: (a) 27 °C, 8 MPa; (b) 35 °C, 8 MPa; (c) 50 °C, 8 MPa; (d) 35 °C, 6 MPa; (e) 35 °C, 10 MPa.

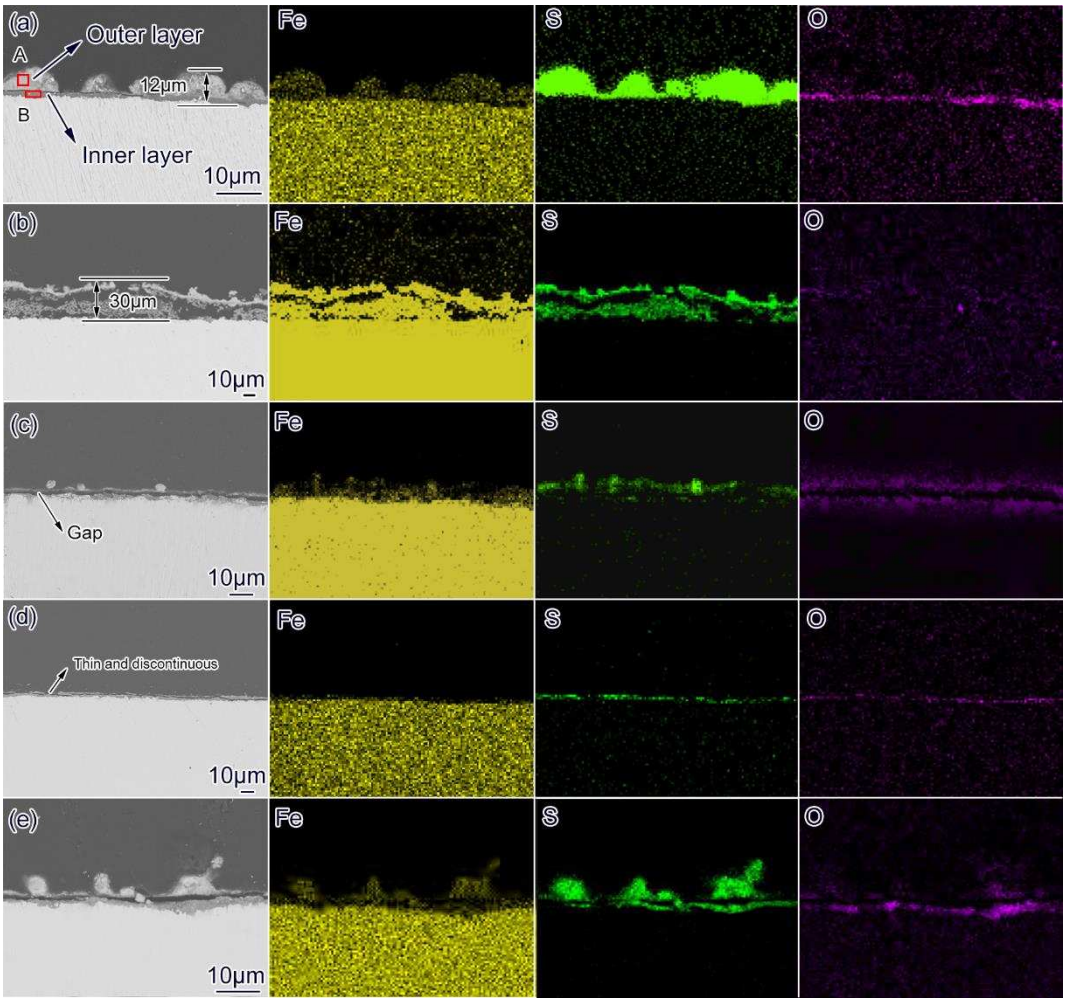

Fig.7. Cross-section backscattered electron morphologies and EPMA mapping images of X65 steel after corrosion in water-saturated supercritical CO_2 system containing 1000 ppmv H_2S impurity: (a) 27 °C, 8 MPa; (b) 35 °C, 8 MPa; (c) 50 °C, 8 MPa; (d) 35 °C, 6 MPa; (e) 35 °C, 10 MPa.

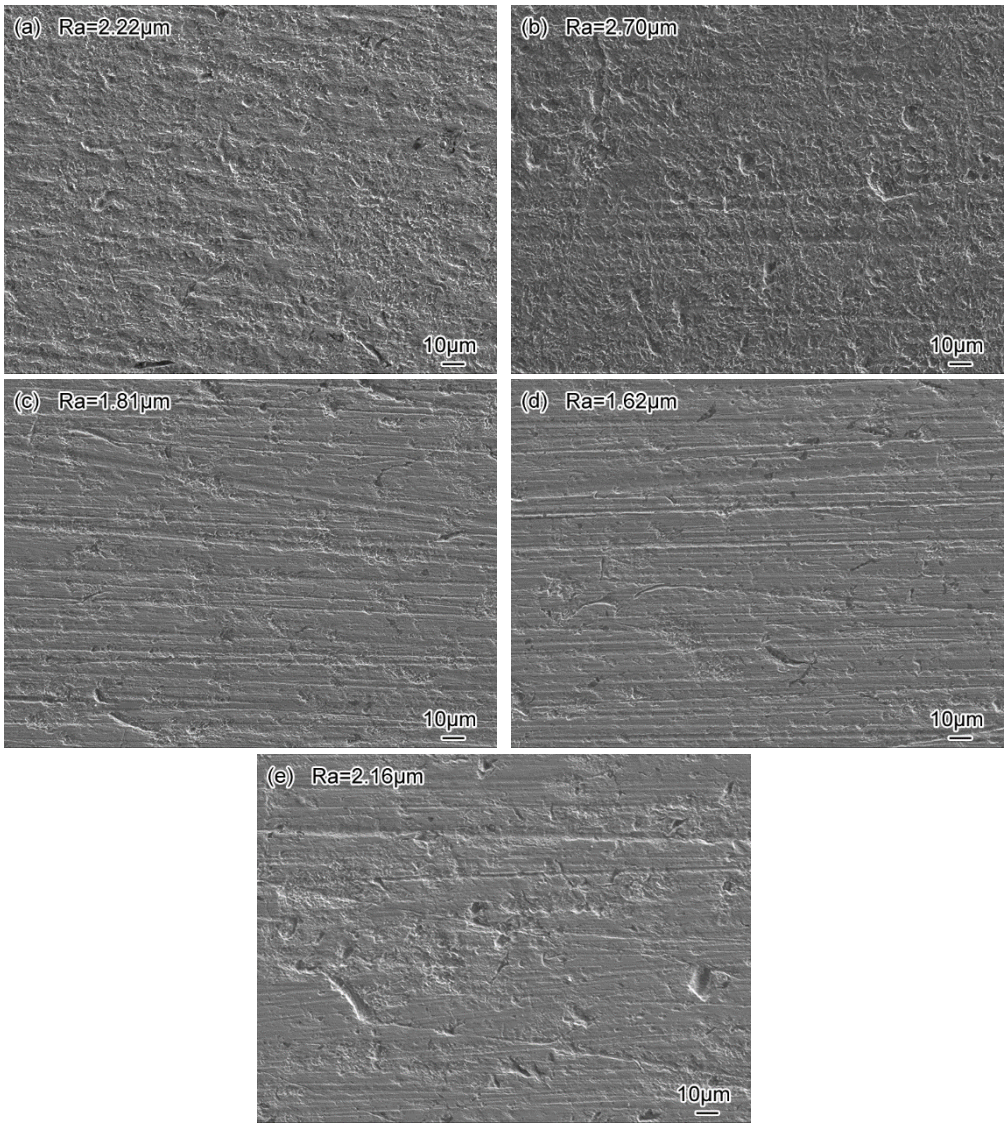

Fig.8. SEM images and surface roughness of X65 steels (after removal of the corrosion products) exposed to water-saturated CO_2 environments at different temperature and pressure in the presence of 1000 ppmv H_2S for 72 h: (a) 27 °C, 8 MPa; (b) 35 °C, 8 MPa; (c) 50 °C, 8 MPa; (d) 35 °C, 6 MPa; (e) 35 °C, 10 MPa.

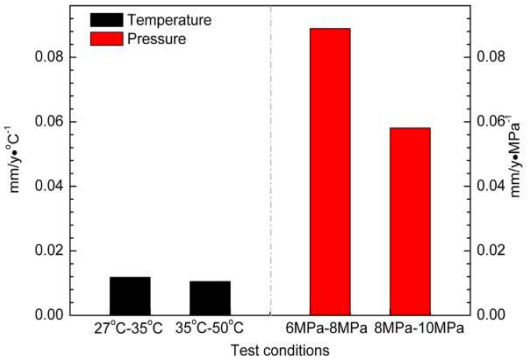

Fig.9. Corrosion rate variations of X65 steel with the change of temperature and pressure.

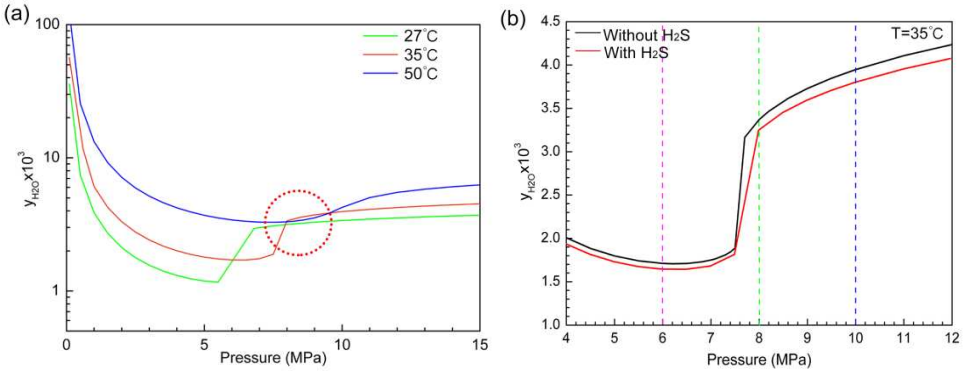

Fig.10. Solubility (mole fraction) of H_2O in CO_2 phase as a function of pressure and temperature: (a) under different temperature with 1000 ppmv H_2S impurity; (b) at 35 °C with and without 1000 ppmv H_2S impurity.

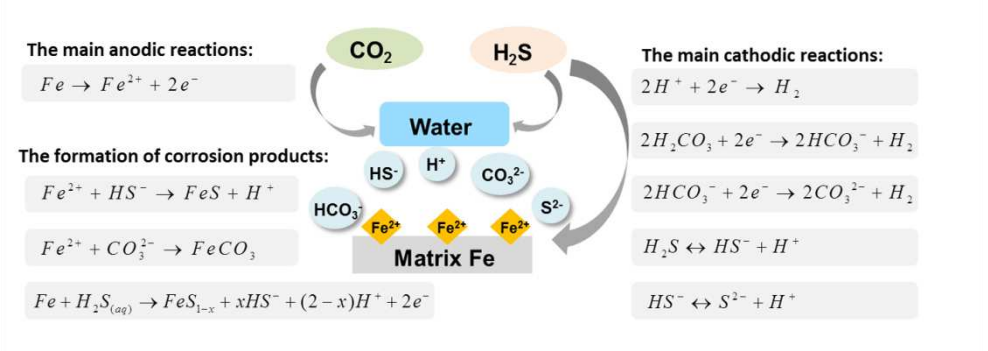

Fig.11. Main corrosion reactions for X65 steel in supercritical CO_2-H_2O-H_2S system.

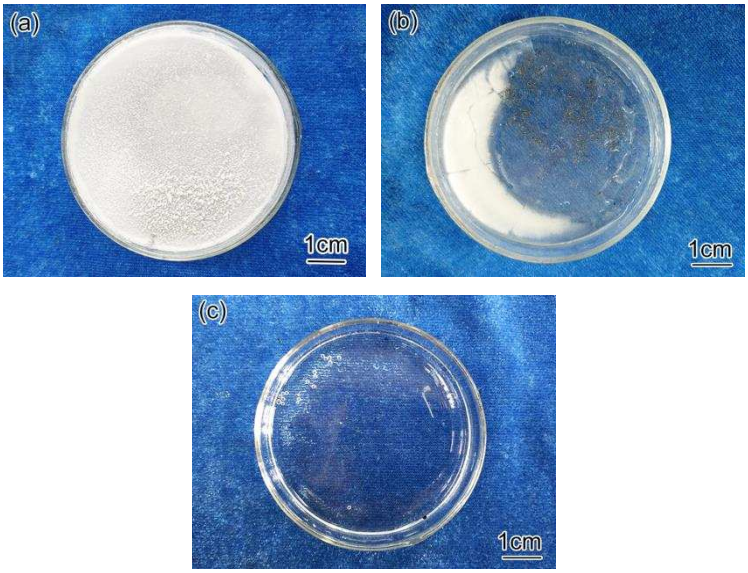

Fig.12 The images of experimental water after finishing test: (a) 27 °C, 8 MPa; (b) 35 °C, 10 MPa; (c) 35 °C, 6 MPa; 35 °C, 8 MPa; 50 °C, 8 MPa.

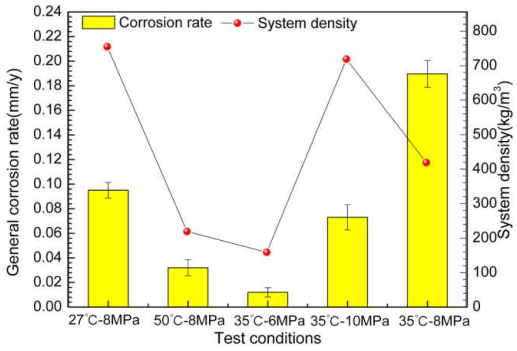

Fig.13. Corrosion rates of X65 steel and system densities under different test conditions.

Table 1 Summary of corrosion research of CO_2 transport pipeline in supercritical CO_2 system with impurities

Materials	T (°C)	P (MPa)	Impurity	Water content	Corrosion rate (mm/y)	Reference
X65	4/50	10	SO_2,H_2S,NO_2,O_2	500ppm	0.005-0.82	Brown et al., 2014
X65	50	4/6/8	None	400ml	0.2-0.4	Choi and Nesic, 2011
CS,1Cr,3Cr	80	8-12	H_2S	100ppm, 10g	＜0.01-0.41	Choi et al., 2015
X65	25/50	8	SO_2	650ppm	0-0.1	Farelas et al., 2013
X65	35/50	8	None	300ppm-3g	0-0.10	Hua et al., 2014
X65	50	10	SO_2,H_2S,NO_2,O_2	10g	0.45-1.16	Sun et al., 2017
X70	25-93	10	SO_2	5g	1.10-3.06	Xiang et al., 2013a
X70	50	10	SO_2,O_2	3g	0.73-1.95	Xiang et al., 2013b
X60,X65,X70,X80	50	8/10/12	SO_2,O_2	1600-3000ppm	0.02-0.94	Xu et al., 2016a
X70	50	10	SO_2,O_2	RH 45-100%	0.03-1.78	Xu et al., 2016b

Table 2 Test conditions.

Test	Temperature (°C)	Pressure (MPa)	H_2O	H_2S	Test time (h)
Liquid CO_2	27	8	Saturated	1000 ppmv	72
	35	6	(10g)		
Supercritical CO_2	35	8	Saturated	1000 ppmv	72
	35	10	(10g)		
	50	8			

Table 3 EPMA analysis of the corrosion scales in region A-F labeled in Fig. 5 (atom percent, %).

Region	Fe	S	C	O
A	54.48	6.04	16.35	23.13
B	49.14	50.86	-	-
C	24.88	4.76	28.79	41.58
D	52.32	47.68	-	-
E	26.87	5.06	17.27	50.81
F	49.06	50.94	-	-

Table 4 EPMA analysis of the corrosion scales in region A and B labeled in Fig. 7 (atom percent, %).

Region	Fe	S	C	O
A	50.59	49.41	-	-
B	23.77	4.94	17.20	54.09

Table 5 Calculated data in the different test conditions in a 3 L autoclave.

Conditions	27 °C-8 MPa	35 °C-8 MPa	50 °C-8 MPa	35 °C-6 MPa	35 °C-10 MPa
Density (kg/m^3)	755.04	419.09	219.40	158.97	719.03
Water in CO_2 (ppm)	3072	3246	3186	1651	3795
Water in CO_2 (g)	2.85	1.67	0.86	0.32	3.35

*Note: The H_2S impurity is in very small amount in the corrosion system compared with CO_2, so it can be ignored when calculating system density.